Sliding friction on particle filled epoxy

Sliding friction on particle filled epoxy: Developing a quantitative model for complex coatings

Sam Krop[a], Han E.H. Meijer[a], Lambèrt C.A. van Breemen[a,*]

[a]*Polymer Technology, Department of Mechanical Engineering, Eindhoven University of Technology, PO Box 513, 5600 MB Eindhoven, The Netherlands*

Abstract

Epoxy resins represent an important class of thermosetting polymers that are extensively used in demanding applications like in scratch resistant coatings. Usually fillers, either hard (inorganic) or soft (rubbery), are added. Here we test hard and soft particle-filled epoxy systems in single asperity sliding friction experiments, and analyze the results with the hybrid numerical-experimental approach presented earlier. The focus is on the detailed modeling of the local deformation processes and it is confirmed that a rate-independent friction model proves appropriate to quantitatively model this complex process. The constitutive framework developed for amorphous thermoplastic polymers adequately describes also these thermoset systems. The materials response during scratching is likewise. Hard fillers decrease the penetration of the indenter into the surface, and consequently enhance scratch resistance; they cause the lateral friction force to decrease, since less material flows in front of the indenter tip. Soft fillers increase the penetration into the surface, according to expectations, but surprisingly also decrease the friction force.
Simulations do not predict this, and suggest an alternative explanation. Migration of rubber particles during sample preparation to the surface could have occurred. Adding a thin rubbery layer to the surface makes the model quantitative, but SEM and TEM pictures of the cross-sections do not confirm this phase separation and instead show the presence of a large number of very small voids. Including these voids in the modeling allows to predict the penetration depth into the surface and lateral force quantitative for all sliding speeds.

Keywords: Sliding friction; Contact mechanics; Solid mechanics; Polymer-matrix composite; Scratch testing; Finite element modeling

1. Introduction

Apart from polyesters also epoxy-based resins are commonly used in scratch resistant coatings. Investigating the scratch and wear resistance of materials is challenging because of the complex contact conditions that involve many variables [1, 2, 3, 4]. Here we focus on the single-asperity sliding friction test, often referred to as 'scratch test', to create well-defined contact situations. Friction is the resistance between surfaces in relative motion. Therefore, a proper description of the real contact area between the two bodies is key. Historically this contact area is approximated by the projected area resulting from either ideal elastic or ideal plastic deformation, or a combination thereof [1, 5, 6, 7], but for visco-elastic materials such as polymers this is a strong assumption. We employ a hybrid experimental–numerical approach instead and started to analyze the scratch response of a model polymer, polycarbonate (PC) [8]. Subsequently, the scratch response of soft and hard particle-filled PC [9] was investigated. The material parameters in the homogenized macroscopic constitutive equation used were computed using Three-Dimensional Representative Volume Elements (3D-RVEs), for details see Krop et al. [10]. The scratch response, including its

*Corresponding author
Email address: l.c.a.v.breemen@tue.nl (Lambèrt C.A. van Breemen)

rate dependence, proved to originate from the materials' intrinsic mechanical response.

For practical coating applications thermoplastic systems such as (particle-filled) polycarbonate are irrelevant since thermosets dominate. Therefore, in this paper we extend our modeling of the scratch test to the standard epoxy that was already quantitatively characterized in [11]. In coating applications fillers are incorporated, hard (inorganic) ones as colorants or stiffness and scratch reinforcements; soft ones to improve the inherently low toughness and impact resistance of the epoxies used, and to relieve residual stresses that originate from the curing process and that could cause warpage and early fracture. This study aims to quantitatively relate the intrinsic mechanical properties of particle-filled epoxy systems to their response in sliding friction.

2. Experimental

2.1. Materials and sample preparation

The matrix material under investigation is Epon 828, kindly provided by Hexion Inc., which is cured with a Jeffamine D230 curing agent, supplied by Huntsman Performance Products. The soft particle core-shell rubbers (CSR), with a size of 0.1–3 µm, are provided as a 40 wt% master batch, i.e. Albidur EP2240-A from Evonik Hanse GmbH. To obtain the 10 vol% CSR-samples used in this study, the Albidur EP2240-A is diluted with the Epon 828 and successively mixed in a stoichiometric ratio with the Jeffamine D230 hardener. For the 10 vol% hard particle filled system we used TiO_2 (Ti-Pure R-706 from DuPont Titanium technologies). First the Epon 828 is stoichiometrically mixed the Jeffamine D230 and in turn the TiO_2 is added in a 90/10 vol% epoxy/TiO_2 ratio. For more details on the sample preparation see Krop et al. [11].
The scratch test samples are prepared in silicone-rubber containers (10 mm × 10 mm area). A 2 mm layer of either the unfilled, hard- or soft filled epoxy, is poured in the mold, degassed in vacuum, and cured. The scratch tests are performed on the free surface of these samples. The batches for the compression tests are cured in aluminium cups with a diameter of 45 mm and 30 mm in height, from which cylindrical samples (⌀ 5 mm × 5 mm) are machined. Both the scratch test and compression samples are cured for two hours at 85°C, with a final cure at 125°C for three hours. The curing quality is checked by differential scanning calorimetry on a Mettler Toledo DSC823e and resulted in a glass-transition temperature of approximately 85°C for all samples, which corresponds to our previous work [11].

2.2. Testing

The scratch samples are tested on a Nano Indenter XP (MTS Nano-Instruments, Oak Ridge, Tennessee) equipped with the option to measure the lateral force. All measurements are performed at a constant normal load where the scratch velocity is varied, but kept constant during a single measurement, from 0.1–100 µm/s. The tip we used is cone shaped an has a top angle of 90° and a top radius of 50 µm. The influence of vibrations are prevented by mounting the indenter on a vibration isolation table and where the temperature and acoustic disturbances are prevented by an enclosing cabinet.
The compression samples are tested on a Zwick 1475 tensile tester in compression set-up. The sample is placed on lubricated (Griffon PTFE spray TF 089) parallel arranged flat steel plates and compressed at a constant true-strain rate of 10^{-3} s^{-1}. To reduce friction between sample and steel plates even further a thin PTFE film (3M 5480 skived plastic film tape) is applied to both ends of the cylindrical sample. All experiments are performed at room temperature.

2.3. Experimental results

Intrinsic response

Figure 1 shows the stress-strain responses of the unfilled epoxy sample and the two particle-filled samples, measured at a constant compressive strain rate of 10^{-3} s^{-1}. Interestingly, the intrinsic mechanical response of these thermosetting polymer systems is almost identical to those of their well-studied amorphous thermoplastic counterparts. We find a non-linear viscoelastic response

up to yield, followed by strain softening and subsequent strain hardening. Furthermore, the addition of 10 vol% soft SR fillers results in a substantial decrease in yield stress, i.e. the first maximum upon loading, while the stress decrease to a local minimum after yield (strain softening) is less pronounced. Adding 10 vol% TiO_2 particles results in a slightly increased yield stress and interestingly, similar to the SR filled sample, a substantially reduced strain softening. Upon

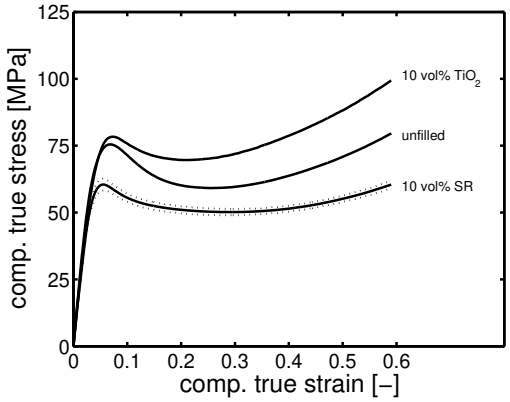

Figure 1: Stress-strain response of unfilled and particle-filled epoxy in uniaxial compression at a strain rate of 10^{-3} s^{-1}.

further loading, the strain hardening regime is entered. Hard fillers increase the large-strain stress-response, soft fillers decrease the response here. The SR-filled samples showed slightly more scatter in the stress-strain response, compared to the unfilled and TiO_2-filled samples, indicated by the dotted lines in Figure 1.

Scratch response

The scratch response at 0.1 µm/s is shown in Figure 2. The lines representing the measurements are the average of at least 3 consecutive experiments with identical input parameters. In

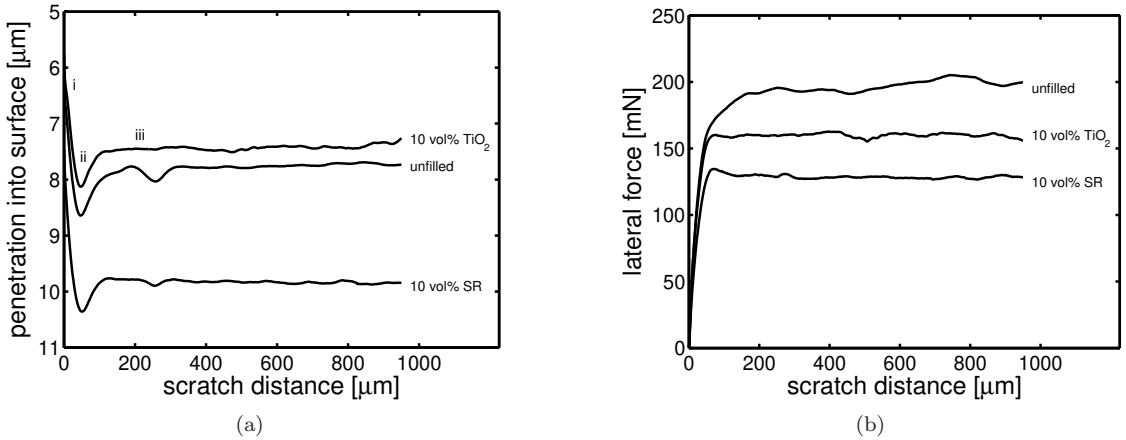

(a) (b)

Figure 2: Penetration into the surface (a) and lateral friction force (b) as a function of scratch distance for unfilled epoxy, and epoxy filled with TiO_2- or SR-particles. Scratch velocity is 0.1 µm/s and normal force applied is 300 mN.

the penetration into the surface (Figure 2a), three points of interest are observed: (i) initial indentation, (ii) with the onset of sliding the contact area decreases, given the constant normal load, this can only result in an increased penetration depth, finally, a stable state (iii) was obtained after the switch-on phenomenon with a lower penetration depth due to the formation of a bow

wave, generating contact surface, in front of the sliding indenter-tip. Qualitatively, the effect of embedding filler particles in the epoxy matrix on the surface penetration is as expected. The hard TiO_2-fillers increase the resistance against deformation, resulting in a decreased penetration depth, whereas this resistance is decreased by the soft SR-particles, resulting in an increase in penetration, similar to our findings in [9]. Quantitatively, however, the influence of the soft rubbery particles appears much stronger compared to that of the hard TiO_2-particles. The effect of these fillers on the lateral-force response, see Figure 2b, is really surprising and much less straightforward to interpret. Since with hard fillers the penetration has decreased compared to unfilled epoxy, a smaller contact area between the two bodies results. As a consequence, the lateral force decreases, despite the higher resistance to deformation of this material. This rationale implies that the lateral friction of the SR-filled sample would increase considerably, since this is also the case for the surface penetration. Clearly this is not the case: the lateral force shows an extensive decrease, even compared to the TiO_2-filled sample. The steady state response (region iii) shows the

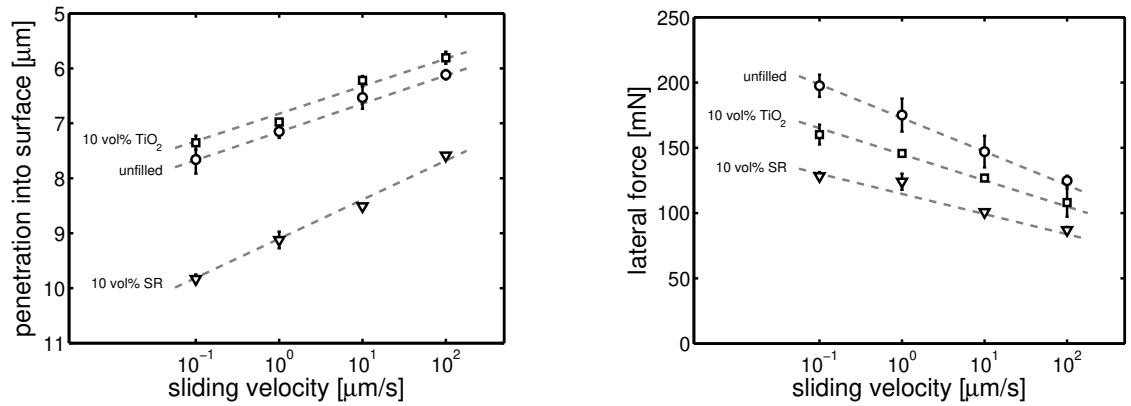

(a) (b)

Figure 3: The mean of the steady-state penetration into the surface (a) and lateral friction force (b) as a function of scratch velocity for unfilled epoxy, and epoxy filled with TiO_2- or SR-particles.

same linear dependence on the logarithm of the sliding velocity applied, see Figure 3, as observed earlier for unfilled and particle-filled polycarbonate [8, 9]. This linear dependence originates from the visco-elastic nature of these polymers, shown by a linear dependence of their yield stress on the logarithm of the strain rate. The addition of filler particles results in a vertical shift of the penetration into the surface only, see Figure 3a, the velocity-dependence itself is unaffected [9]. This is also the case for the lateral friction force, see Figure 3b.

3. Modeling

3.1. Intrinsic mechanical response

Constitutive model

The constitutive model used is the Eindhoven Glassy Polymer (EGP) model. A full description of the model in all its detail can be found in Klompen et al. [12] and Van Breemen et al. [13]. In these papers also the complete procedure can be found on how to characterize a material and determine the model parameters. The fundamentals of the EGP model are included in this manuscript to facilitate the reader and are not part of the actual research.

The basis is the additive decomposition of The Cauchy stress into a hardening stress $\boldsymbol{\sigma}_r$ and a driving stress $\boldsymbol{\sigma}_s$:

$$\boldsymbol{\sigma} = \boldsymbol{\sigma}_r + \boldsymbol{\sigma}_s. \tag{1}$$

Where $\boldsymbol{\sigma}_r$ accounts for the stress contribution of the network and is modeled with a neo-Hookean spring with hardening modulus G_r:

$$\boldsymbol{\sigma}_r = G_r \tilde{\boldsymbol{B}}^d. \tag{2}$$

The driving stress, $\boldsymbol{\sigma}_s$, itself is additively decomposed into a hydrostatic part ($\boldsymbol{\sigma}_s^h$) and a deviatoric part ($\boldsymbol{\sigma}_s^d$), modeled as a combination of n parallel linked Maxwell elements:

$$\boldsymbol{\sigma}_s = \boldsymbol{\sigma}_s^h + \sum_{i=1}^{n} \boldsymbol{\sigma}_{s,i}^d = \kappa(J-1)\boldsymbol{I} + \sum_{i=1}^{n} G_i \tilde{\boldsymbol{B}}_{e,i}^d, \tag{3}$$

with bulk modulus κ, volume change ratio J, unity tensor $\boldsymbol{I}$, shear modulus G, and the elastic part of the isochoric left Cauchy-Green strain tensor $\tilde{\boldsymbol{B}}_e^d$. The specific modes are denoted by subscript $i = [1, 2, ..., n]$.

Via a non-Newtonian flow rule, the modal plastic deformation rate tensors $\boldsymbol{D}_{p,i}$ are related to the modal deviatoric driving stresses $\boldsymbol{\sigma}_{s,i}^d$:

$$\boldsymbol{D}_{p,i} = \frac{\boldsymbol{\sigma}_{s,i}^d}{2\eta_i(\bar{\tau}, p, S_a)}. \tag{4}$$

The modal viscosities η_i depend on the total equivalent stress $\bar{\tau} = \sqrt{\frac{1}{2}\boldsymbol{\sigma}_s^d : \boldsymbol{\sigma}_s^d}$, the hydrostatic pressure p and the thermodynamic state of the material S_a. The viscosities are modeled by a modified Eyring flow rule [14]:

$$\eta_i = \eta_{0,i,ref} \frac{\bar{\tau}/\tau_0}{\sinh(\bar{\tau}/\tau_0)} \exp\left(\frac{\mu p}{\tau_0}\right) \exp\left(S_a R(\bar{\gamma}_p)\right), \tag{5}$$

where the initial viscosities $\eta_{0,i,ref}$ define the so-called reference (un-aged) state. With τ_0 the characteristic stress, μ the pressure dependence and S_a representing thermodynamic state of the material. Strain softening is described by the function $R(\bar{\gamma}_p)$. The equivalent plastic strain $\bar{\gamma}_p$ follows from its evolution equation:

$$\dot{\bar{\gamma}}_p = \sqrt{2\boldsymbol{D}_p : \boldsymbol{D}_p}. \tag{6}$$

The EGP model is implemented via the user subroutine HYPELA2 in the FEM package MSC.Marc. The model parameters are summarized in Table A.1, denoted as set 1, with the reference spectrum in Table A.2. Figure 4a shows the quantitativeness of model predictions at all different strain rates applied using this parameter set. The material's thermodynamic state is captured with $S_a = 17.7$. Figure 4b shows the model response for different values of S_a compared to the experiments at a strain rate of 10^{-3} s^{-1}.

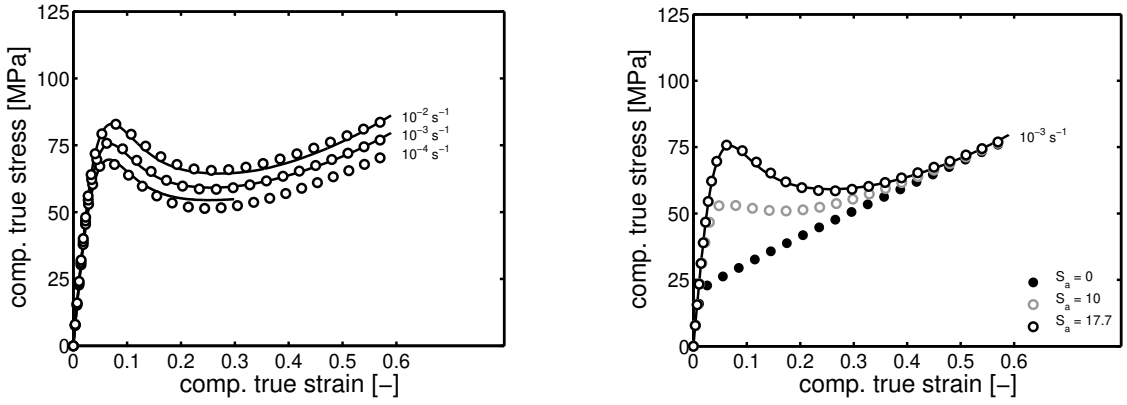

(a) (b)

Figure 4: Stress-strain response of unfilled epoxy at (a) different strain-rates applied (solid lines), compared to model predictions using parameter set 1 (open ymbols), and at (b) 10^{-3} s^{-1} strain-rate compared to model predictions using different values of S_a.

Homogenization procedure

The homogenization procedure used to obtain the material parameters for the particle-filled epoxy samples is described in full detail in Krop et al. [9]. This method uses a combination of numerical simulations and experimental compression data. Full three-dimensional representative

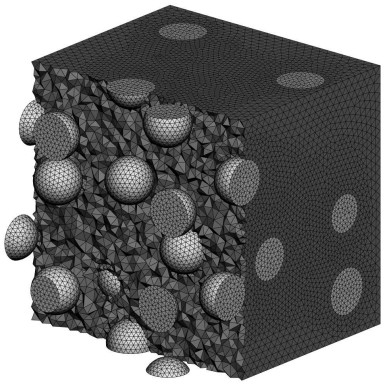

Figure 5: Example of a meshed RVE with part of the matrix made invisible.

volume elements (3D-RVEs), periodic cubic unit cells containing 32 particles, are used as a simplified model for the heterogeneous micro-structure. Particles are assumed spherical, mono-sized, and adhere perfect to the epoxy matrix. A finite element mesh of the 3D-RVE is generated, an example of which is shown in Figure 5, and material properties are assigned. Simulations are performed in both uniaxial tension and compression loadings at different strain rates, to obtain homogenized material parameters. Figure 6a shows the stress-strain response of these RVEs in compression at 10^{-3} s^{-1} strain rate (closed black symbols), obtained using parameter set 1 for the epoxy matrix, while the TiO_2 particles are modeled as a linear elastic material ($E = 230$ GPa and $\nu = 0.27$) and the rubber particles are modeled neo-Hookean ($G = 5$ MPa), compared to experimental results as shown in Figure 1. In the homogenization procedure the stress-strain responses that result from these RVE simulations is fitted using the Equations (1) and (3)–(5) to provide values for τ_0, μ and G_r, while the transverse deformation of the RVE provides the Poisson's ratio ν. From the Poisson's ratio, the elastic bulk modulus κ is determined using the elastic conversion

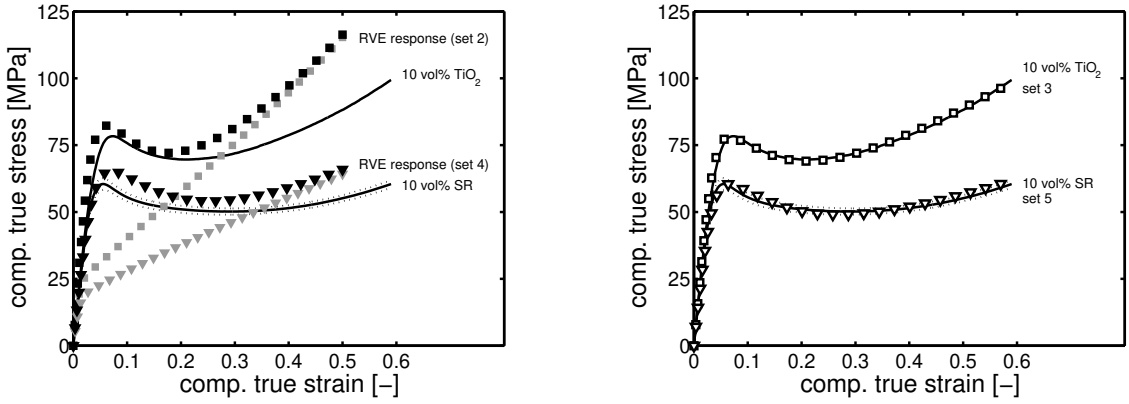

(a) (b)

Figure 6: (a) Stress-strain response of epoxy filled with either 10 vol% TiO_2 or 10 vol% rubber, at a strain rate of 10^{-3} s^{-1}. Lines are experimental results as in Figure 1, compared to predictions from FE-simulation of 3D-RVEs using either $S_a = 17.7$ (closed black symbols) or $S_a = 0$ (closed gray symbols) for the epoxy matrix. (b) Same as (a), but here experiments are compared to model predictions resulting from the homogenization procedure, where parameters are adapted to the large-strain experimental response as described in the text (open symbols)

formula

$$\kappa = \frac{E}{3(1-2\nu)}, \tag{7}$$

where the Young's modulus E is obtained from the initial slope of the stress-strain response. The reference state of the filled samples results from simulations with $S_a = 0$, as in Figure 4b, for the epoxy matrix (closed gray symbols in Figure 6a). The relaxation spectra are subsequently established using this set of input-parameters, following the procedure described in [13]. This results in parameter set 2 for TiO_2-filled epoxy and set 4 for SR-filled epoxy (see Table A.1). Clearly, these parameter sets fail to correctly describe the experimental data (solid lines). The discrepancy is attributed to an accumulation of damage in the systems, which is not taken into account in the simulations, and a difference in aging kinetics of the polymer matrix as a result of matrix-filler interactions [10, 11]. Following the same procedure as used in Krop et al. [9], the material parameters, specifically G_r and S_a, are adapted such that the experimentally obtained response is captured, see Figure 6b (open symbols). This leads to adapted parameter sets for both TiO_2-filled epoxy (set 3) and SR-filled epoxy (set 5). All the material parameters are summarized in Table A.1. In the remainder, unless specified otherwise, we will use parameter set 1 for unfilled epoxy, set 3 for TiO_2-filled epoxy, and set 5 for SR-filled epoxy. The relaxation spectra of the filled samples are summarized in Tables A.3 and A.4.

3.2. Scratch simulations

FE-mesh and friction modeling

Because the material response is isotropic and the indenter tip is rotation symmetric only half of the actual volume has to be meshed. The indenter tip is modeled as an impenetrable surface with infinite stiffness. The size of the polymer-material geometry is chosen such that the edges do not influence the stress fields in the simulations which results in a total volume of $0.2 \times 0.2 \times 0.8$ mm^3. The final mesh is shown in Figure 7. To reduce computation time a local automatic mesh adaptivity criterion is used, which is a built-in function of the finite element program MSC.Marc, resulting in 73,088 linear brick elements. Since the geometries are specified this only leaves the boundary conditions. The symmetry plane is defined as the x-y-plane, therefore the displacement in z-direction is fixed. The sides are retained in z- and y-direction. Scratching is done from the top x-z-plane and the sliding velocity is defined by moving the polymer geometry in negative x-direction. The indenter-tip geometry contains a control node in which the normal

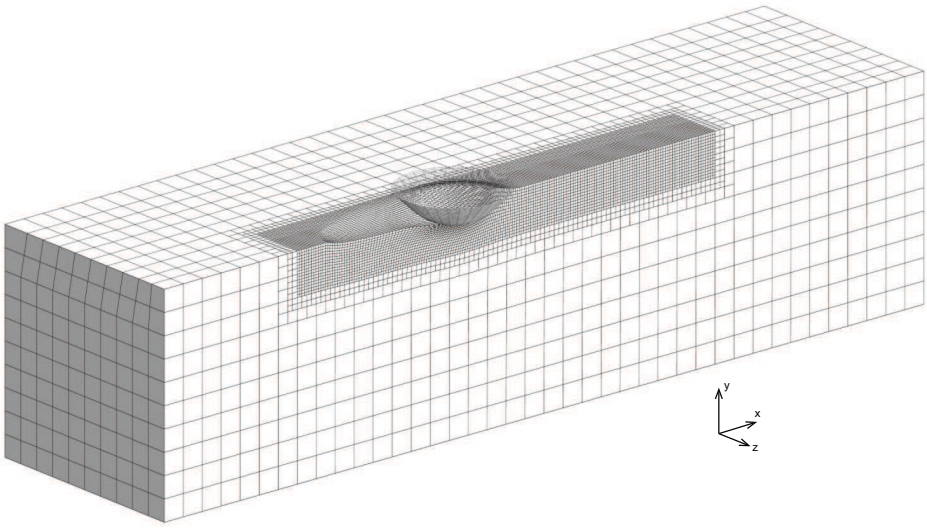

Figure 7: Finite element mesh for the scratch simulations.

force is applied and the x- and z-displacements are fixed. The scratch response is very sensitive to the exact tip geometry [9], an optical profilometer (Sensofar Plu 2300) is used to measure the profile of the indenter tip. This measured profile is used in the simulations.
Local friction is modeled with the most simple model that is implemented in MSC.Marc, Coulomb friction. This model is characterized by a constant, velocity independent, friction coefficient μ_f via:

$$\|\vec{f_t}\| = \mu_f f_n \quad \text{(stick) and} \quad \vec{f_t} = -\mu_f f_n \vec{t} \quad \text{(slip)}, \tag{8}$$

with the tangential (friction) force $\vec{f_t}$, the normal force f_n, the local friction coefficient μ_f, and the tangential vector $\vec{t}$ in the direction of the relative velocity $\vec{v}_r$, defined as:

$$\vec{t} = \frac{\vec{v}_r}{\|\vec{v}_r\|}. \tag{9}$$

The approach of simplifying the friction model and focusing on introducing more complexity in the local deformation processes was successfully used to capture the scratch response of unfilled and hard- and soft-particle filled polycarbonate [8, 9].

3.3. Comparing experiments with simulations

Determining friction coefficient for matrix material

With the material parameters of the particle-filled samples established (parameter sets 1, 3, and 5), scratch simulations are performed. In Krop et al. [9], using the same indenter, a value of $\mu_f = 0.25$ was found to best describe the experimental data of unfilled and filled PC. The procedure of determining μ_f for this specific polymer-indenter combination is repeated with the unfilled epoxy sample, see Figure 8. Here, a slightly higher value of $\mu_f = 0.27$ is necessary to capture the scratch response. This small difference is explained by differences in the surface chemistry between this epoxy system and PC. At the molecular scale, friction is influenced by factors such as the presence and type of chain ends at the polymer surface, bond-breaking of the polymer chains, and surface and subsurface relaxation modes [15, 16]. Since only one μ_f was capable of capturing the responses of both unfilled and particle-filled PC [9], we assume the same here.

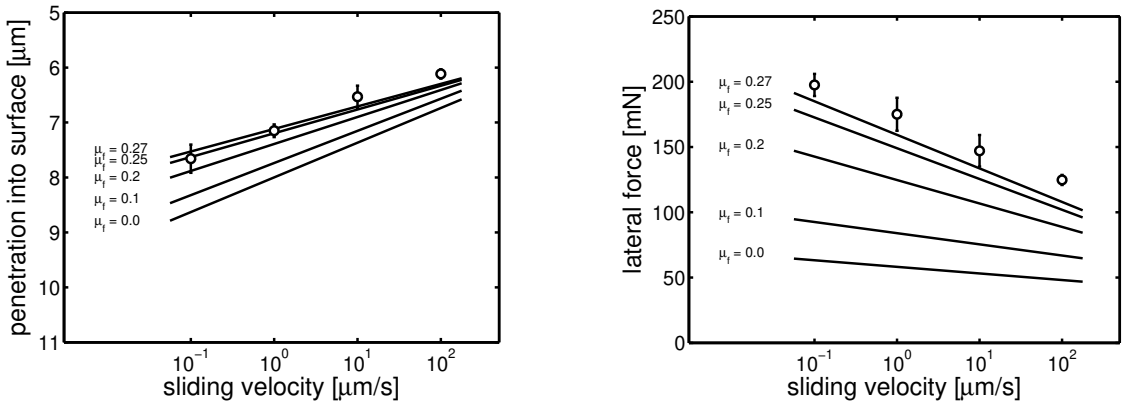

(a) (b)

Figure 8: Penetration into the surface (a) and lateral friction force (b) as a function of scratch velocity at 300 mN normal load applied. Symbols are experimental results of unfilled epoxy, as in Figure 3, and lines are simulation results with different values of μ_f.

Application to particle-filled epoxy

Figure 9 shows the scratch responses obtained from simulations compared to the experimental results for the particle-filled epoxy systems. For TiO_2-filled epoxy the penetration into the surface (Figure 9a) and the lateral friction force (Figure 9b) are quantitatively described by the simulations for all scratch velocities applied. This in large contrast with the predictions for the rubber-filled sample. The simulations underestimate both the absolute penetration into the surface and its dependence on the scratch velocity, see Figure 9a (gray line). The result is a discrepancy of about 15% at the lowest sliding velocity and, interestingly, the velocity-dependence is predicted parallel to that of unfilled and TiO_2-filled epoxy. With a lower predicted penetration depth, resulting in

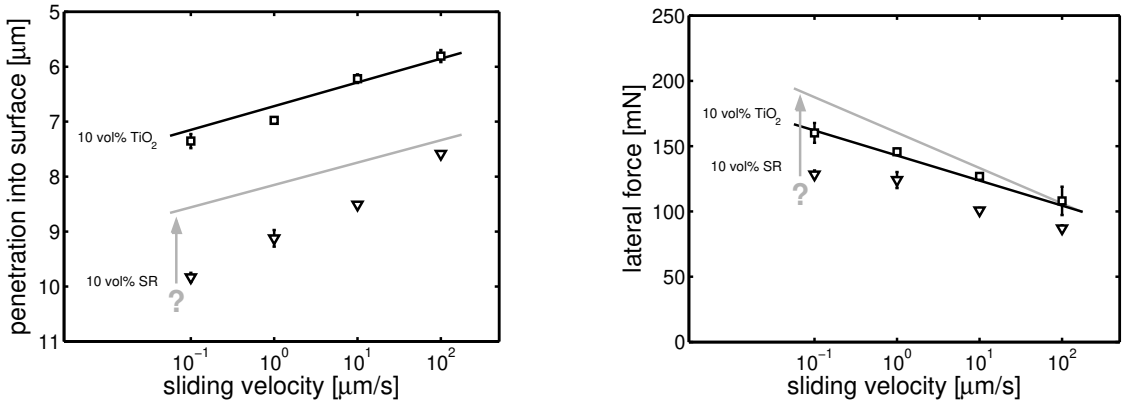

(a) (b)

Figure 9: Penetration into the surface (a) and lateral friction force (b) as a function of scratch velocity at 300 mN normal load applied. Symbols are experimental results, as in Figure 3, and lines are simulation results for TiO_2-filled epoxy (black) and for SR-filled epoxy (gray). All simulations with $\mu_f = 0.27$. Arrows indicate discrepancy between model predictions and experimental results for SR-filled epoxy.

a smaller indenter–substrate contact area, it is expected that the lateral friction force would be underestimated as well. This is clearly not the case, see the gray line in Figure 9b (close to the unfilled line). At the lowest sliding velocity the lateral force is over-predicted with about 50%, and also the decay with increasing velocity is overestimated.

To check whether this discrepancy results from the larger absolute value of the penetration depth

itself, i.e. that it results from shortcomings in our approach (e.g. subtle geometry or surface roughness effects on the indenter cone), both the unfilled and the TiO_2-filled samples are tested at a higher normal load of 500 mN. This results in penetration depths that exceed those of SR-filled epoxy at 300 mN, see Figure 10a. Comparing these experimental results with simulations shows that the TiO_2-filled sample is captured well over the total velocity range. For the unfilled sample the prediction is correct for the highest sliding velocity, while at lower scratch velocities deviations increase. The surface penetration is under-predicted with 1 µm at the lowest speed. This is still a more accurate prediction, 7% off, compared to that of the rubber-filled sample, 15% off, due to the larger absolute penetration depth. Please note that the EGP-model used, does not include its most recent advances, i.e. Bauschinger effect and thermorheological complex behavior [17]. These phenomena become more pronounced when considering very large deformations, e.g. high loads and a large range of locally high strain-rates. Here load reversal and a Ree-Eyring contribution to the flow stress have to be taken into account. Including this in the current manuscript is not feasable as it is a study on its own. In contrast to the rubber-filled sample at 300 mN, the lateral friction force at 500 mN normal load is predicted quantitatively for both samples, see Figure 10b. Comparing these experiments and simulations confirms that our approach does not fail at deeper

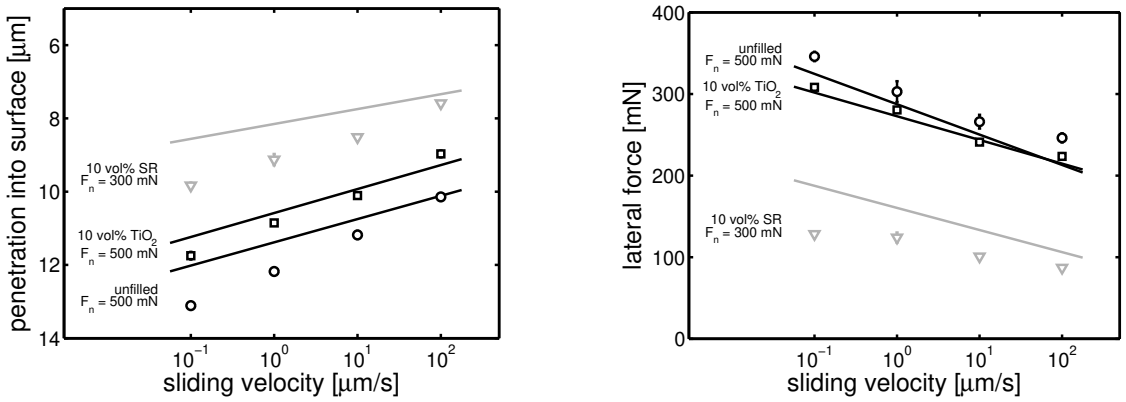

Figure 10: Penetration into the surface (a) and lateral friction force (b) as a function of scratch velocity for unfilled and TiO_2-filled epoxy at 500 mN normal load applied. Experiments (symbols) compared to simulations results using $\mu_f = 0.27$ (solid lines). For comparison, experimental results and numerical predictions of SR-filled epoxy at 300 mN normal load are added in gray.

penetration depths and, therefore, it does not explain the discrepancy between simulations and experiments for the rubber-filled sample.

3.4. Why FE-modeling and experiments are synergetic

Surface interaction

Since the matrix material already affects the value of μ_f needed to capture the response, ($\mu_f = 0.25$ for PC [9] and $\mu_f = 0.27$ for this epoxy system), one explanation could be that the SR-fillers directly influences the surface chemistry, resulting in a different interaction with the indenter tip at the molecular scale. To check this, simulations are performed with different values of μ_f, see Figure 11. A lower value of μ_f has the effect of a less severe bow wave formation in front of the indenter. Since the experiment is force-controlled, a decrease in contact area and, therefore, an increase in penetration depth results, see Figure 11a. Due to the visco-elastic nature of the material, this effect becomes stronger with decreasing sliding velocity. With a single value of $\mu_f = 0.1$ both the absolute penetration depth and its dependence on sliding velocity are captured. With the decreased contact area from lowering μ_f, a decrease of lateral friction force is observed, see Figure 11b. Although lower values of μ_f give better predictions of the lateral force, a single value does not cover both force and penetration depth.

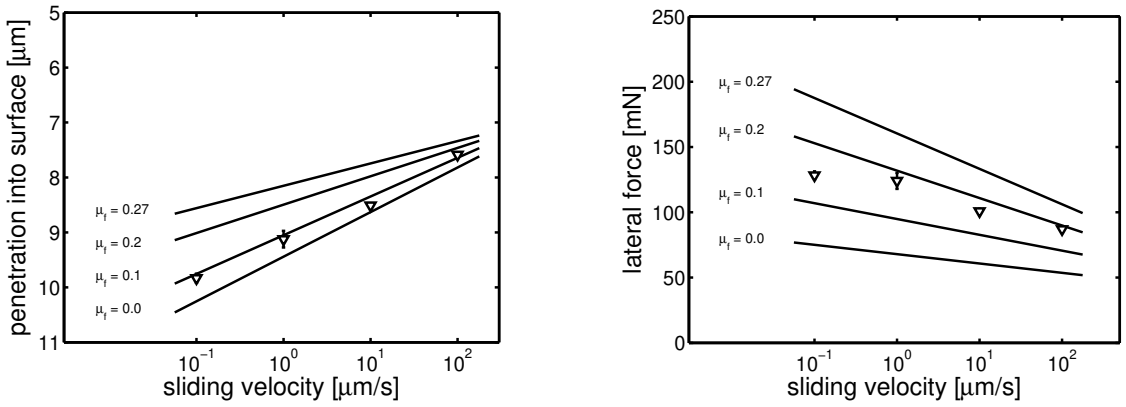

(a) (b)

Figure 11: Penetration into the surface (a) and lateral friction force (b) as a function of scratch velocity for epoxy filled with SR-particles. Experiments (symbols) compared to simulation results using different values for μ_f (lines).

Rubber layer

A second explanation for the discrepancy between simulations and experiments could be a difference in composition of the top layer. Although the samples have been thoroughly mixed during sample preparation, the initial stages of the curing process result in a rapid decrease in viscosity of the uncured resin, increasing the mobility of the filler particles. This may cause the formation of clustered regions and/or that rubber fillers are migrating to the top layer to form a region with higher filler content. The relatively larger scatter observed in the stress-strain response, see Figure 1, could hint to inhomogeneities in composition. To test the influence of a difference in mechanical properties of the surface region, a single layer of 1 µm thick elements is added to the FE-mesh, see Figure 12, and modeled neo-Hookean with a 20 MPa modulus. This thickness is chosen since it is the typical length scale of the filler particles (0.1–3 µm diameter) and the modulus is a compromise between pure rubber properties and epoxy with (extremely) high filler loading. The part underneath this layer is, as before, modeled with parameter set 5. Comparing

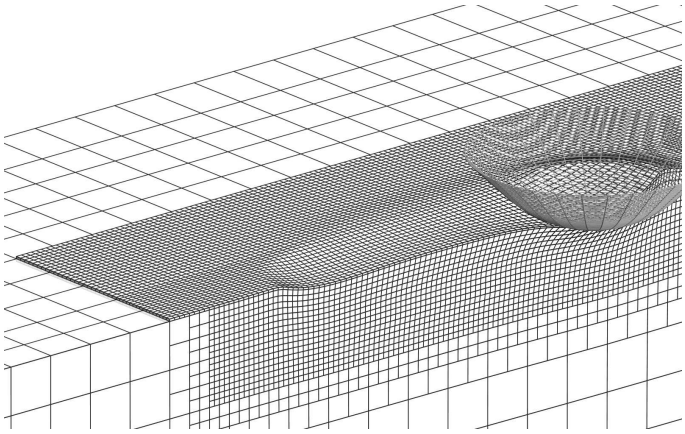

Figure 12: Zoom-in of finite element mesh for the scratch simulations with rubber layer on the scratch surface.

both scenarios, homogeneous composition versus a concentrated rubbery layer with both the same local friction ($\mu_f = 0.27$), the effect of this rubbery layer on the scratch response is considerable, see Figure 13. Initial penetration during the indentation step is unaffected, see Figure 13a, as is the sink-in when sliding commences, but the steady state penetration has increased about 15%. The absolute difference exceeds the 1 µm from the rubber layer itself. Despite this increase in

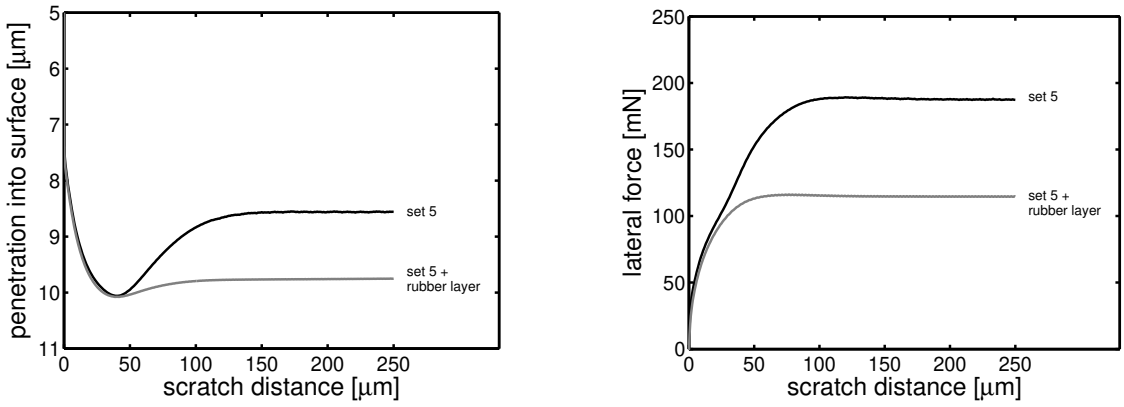

(a) (b)

Figure 13: The effect of the rubber top-layer on scratch response: penetration into the surface (a) and lateral friction force (b) as a function of scratch distance. Simulation results of 300 mN normal load, 0.1 µm/s sliding velocity, with $\mu_f = 0.27$ local friction coefficient.

penetration depth, also the lateral force decreases, by about 40%, see Figure 13b. Comparing

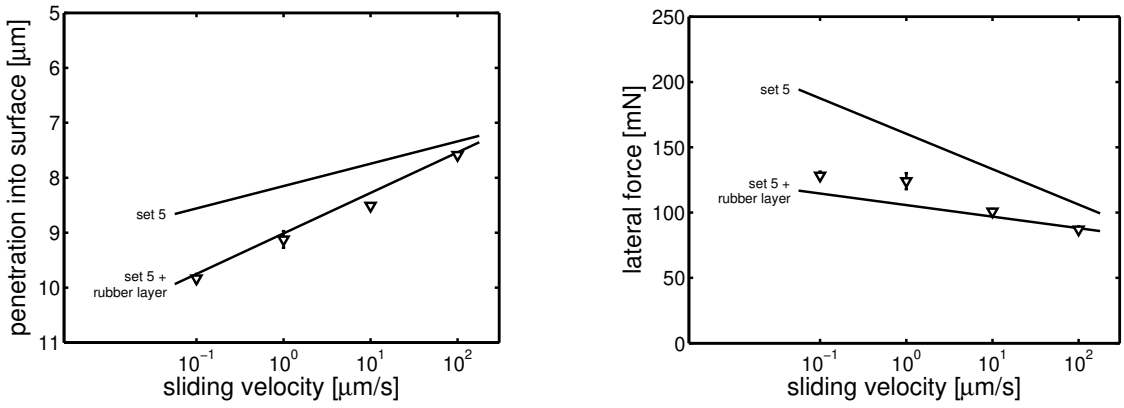

(a) (b)

Figure 14: Penetration into the surface (a) and lateral friction force (b) as a function of scratch velocity for epoxy filled with SR-particles. Experiments (symbols) compared to simulations (solid lines) using $\mu_f = 0.27$ with a homogeneous scratch domain or with a rubber top-layer.

these simulations with experiments yields excellent agreement, see Figure 14.
The reason for the somewhat surprising effect of such a relatively thin, rubbery layer lies in the shape, but more importantly in the composition, of the bow wave that is formed in front of the indenter. This is illustrated in Figure 15, where the cross-section at the symmetry plane is shown for both scenarios: (i) homogeneous material properties throughout the whole (sub)surface (see Figure 15a), and (ii) a rubbery layer on top (see Figure 15b). Here the simulations, 300 mN normal load and 0.1 µm/s sliding velocity, have reached steady-state. The scratch profiles at the symmetry-plane, as indicated by the dashed line for case (i) and the gray line for case (ii), are depicted vertically scaled (2×) in Figure 15c. To compare the contributions from the homogeneous filled part only, the profile of this part in case (ii) is added, depicted as a black solid line. The rubbery layer only transfers the stresses to the epoxy-rich part underneath, its contribution to the lateral force in the top part of the bow wave is minimal. Therefore, we only consider the projected vertical contact height between the indenter and the homogeneous filled part, as shown in Figure 15c. With the top-layer added, clearly a decrease in projected contact height results,

even though the total penetration depth had increased. This difference in contact height may seem small, but it results in a quadratically increased projected contact area due to the cone-shape of the indenter. The rubber layer is acting as a stress-reliever for the material underneath, resulting in a smaller volume of epoxy-dominated material to be loaded.

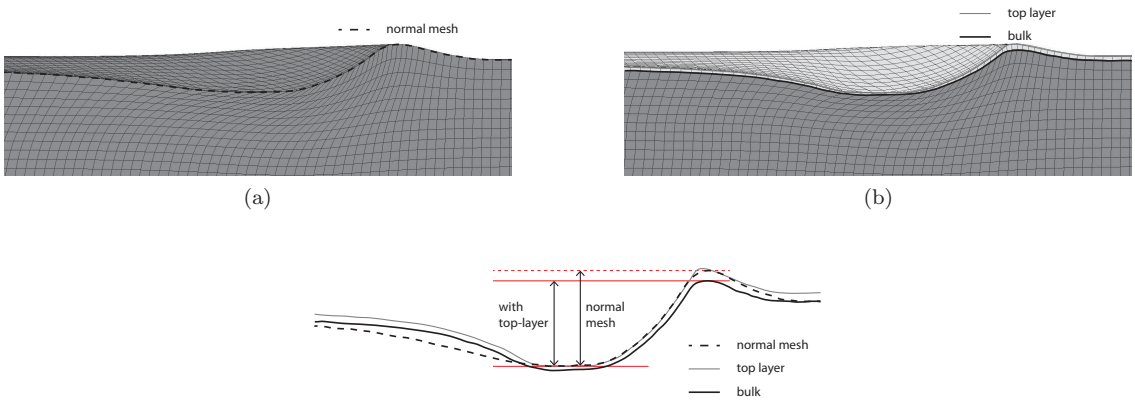

(a) (b)

(c)

Figure 15: Scratch response of rubber-filled epoxy at 0.1 µm/s sliding velocity and 300 mN normal load, (a) with homogeneous material properties (set 5) and (b) with a rubber layer on the same bulk (set 5); scratch-surface profiles are clarified with lines as indicated in the legend; indenter is not shown for clarity reasons. (c) Vertically scaled (2×) scratch profiles from (a) and (b). Profiles are shifted such that homogeneous bulk, indicated by dark gray in (a) and (b), is at the same level. The projected contact area in horizontal direction between indenter tip and homogeneous bulk is indicated by arrows.

Porous structure

A third, and final, explanation is suggested by inspecting the SEM (Figure 16) and TEM (Figure 17) images of cross-sections of the scratch sample. No macroscopic phase separation at the surface is observed. Instead, clearly 200–300 nm sized cavities are present everywhere in the material, both in the surface-layer (Figure 16a and 17a) and throughout the rest of the sample (Figure 16b). In the TEM micrographs, the voids are bright white and the rubber particles are visible as dark-gray regions in the epoxy matrix, see Figure 17b. The origin of these tiny voids is

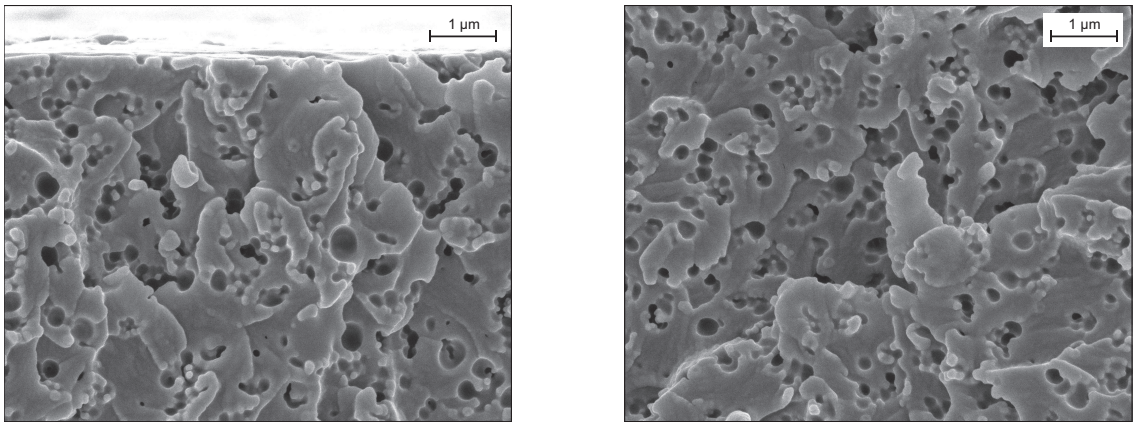

(a) (b)

Figure 16: SEM pictures of 10 vol% rubber-filled epoxy, of cross-sections at (a) the surface and (b) in the middle of the sample.

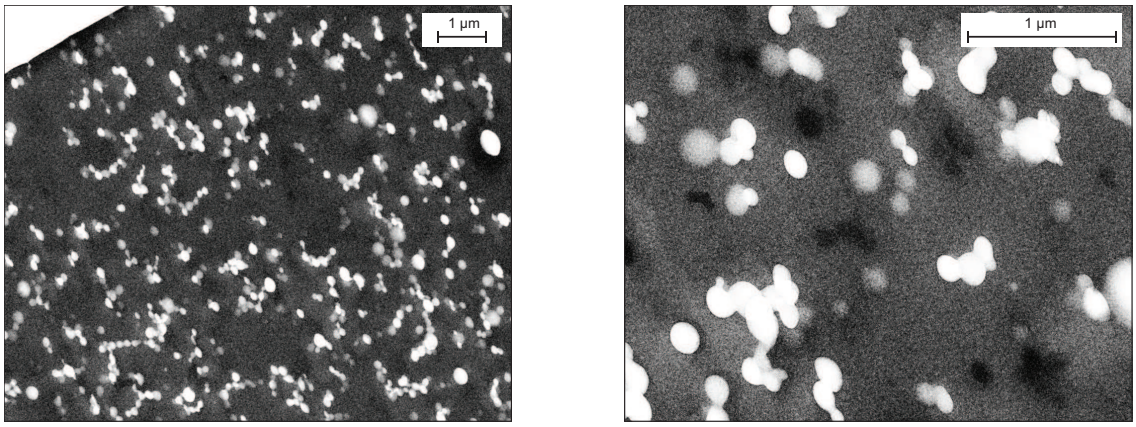

(a) (b)

Figure 17: (a) TEM micrographs of 10 vol% rubber-filled epoxy. The surface is seen in the top-left corner. The micro-voids appear as bright white holes in the matrix and the SR fillers as dark-gray regions, which are better visible in the enlargement (b).

unknown, but they have a definitive impact on the materials behavior. Analyzing the SEM and TEM images gives a void volume fraction of 7–10% and to estimate their effect on the mechanical response, RVEs are generated with 10 vol% holes. The matrix is given the (ideal) homogenized material properties of 10 vol% rubber-filled epoxy (set 4, see Figure 6a). Figure 18a shows the response that results from set 4 (closed symbols), and the resulting stress-strain response of the voided RVEs (open symbols) compared with experiments. Evidently, adding 10 vol% voids yields a stress-strain response of the RVE that agrees already well with the experiments. With voids the compressive stress decreases considerably, compared to the case of only rubber-fillers, set 4 (and 5, see Figure 6b), since 10 vol% of the system does not bear load anymore. The material parameters describing the RVE response of the rubber-filled samples in set 5 were adapted to match the experimental yield- and post-yield response, see Figure 6b, but this, as we see now, was partly done for the wrong reasons –damage rather than voids. Here we keep using the adapted parameter set 5, but change the compressibility, via the bulk modulus κ, to reflect the presence of the voids and, from the lateral dimension change of the RVE of the voided system, a decrease in the value of κ from 3645 MPa to 2700 MPa is found, Table A.1 (set 6). This large difference in κ may seem exorbitant at first, but it originates from only a minor difference in Poisson's ratio ν. For set 4 (rubber-filled epoxy), the transverse macroscopic strain observed in the RVE-simulations gave $\nu = 0.41$, whereas for set 6, $\nu = 0.39$ was found. Assuming that the Young's modulus E did not change, which is obviously not the case, Equation 7 shows that this small difference in ν already leads to a 20% decrease of κ. Since E has actually decreased as well, an even larger decrease of the bulk modulus results. Interestingly, the influence of the bulk modulus κ on the response in uni-axial compression/tension is absent since the material is allowed to freely contract/expand in the plane of loading. This is reflected by an identical stress-strain response for set 5 and 6, see Figure 18b, despite of the 1 GPa difference in bulk modulus.

Scratch simulations are performed using parameter set 6 and $\mu_f = 0.27$. Changing only the bulk modulus, as compared to set 5, results in a considerable decrease in penetration depth, see Figure 19a. In the scratch experiment, κ clearly has a major impact. Below the indenter and directly in front of it, in the bow wave, the material undergoes confined compression, resulting in a high sensitivity to the volumetric contribution. Interestingly, the lateral friction force decreases with the higher penetration depth, see Figure 19b, which indicates that the bulk modulus strongly influences the resistance of the material in the bow wave. Compared to the experimentally obtained response, set 6 still underpredicts both penetration depth and lateral friction force. Therefore, we explore the influence of decreasing κ further and perform simulations using $\kappa = 2200$ MPa

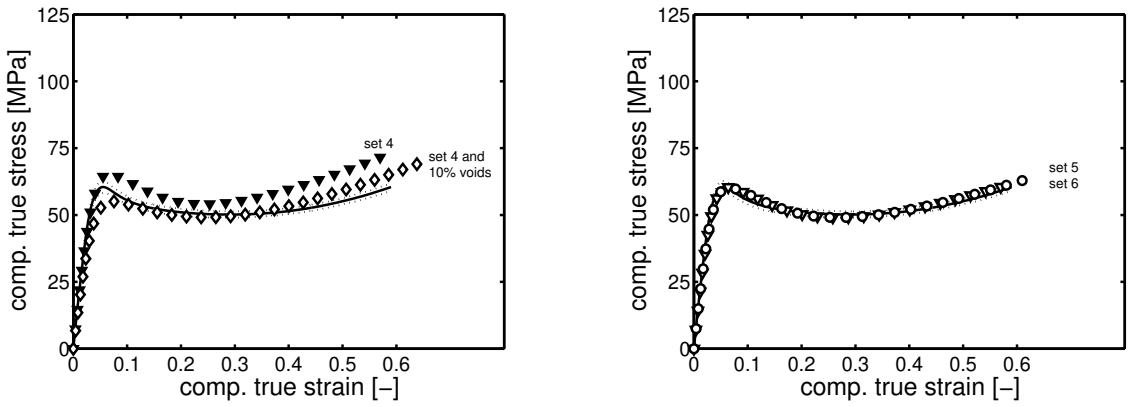

(a) (b)

Figure 18: Stress-strain response of epoxy filled with 10 vol% rubber at a strain rate of 10^{-3} s^{-1}. Solid black lines are the mean experimental results and dotted lines give the scatter, compared to (a) simulations using parameter set 4 (ideal rubber-filled, no voids, closed symbols), and simulations of RVEs with 10 vol% voids (open symbols) where the matrix is described by parameter set 4, and compared to (b) model predictions using to the large strain response of the experiments (G_r) adapted homogenized parameter set 5, and one last identical set with a to voids adapted bulk modulus κ: parameter set 6.

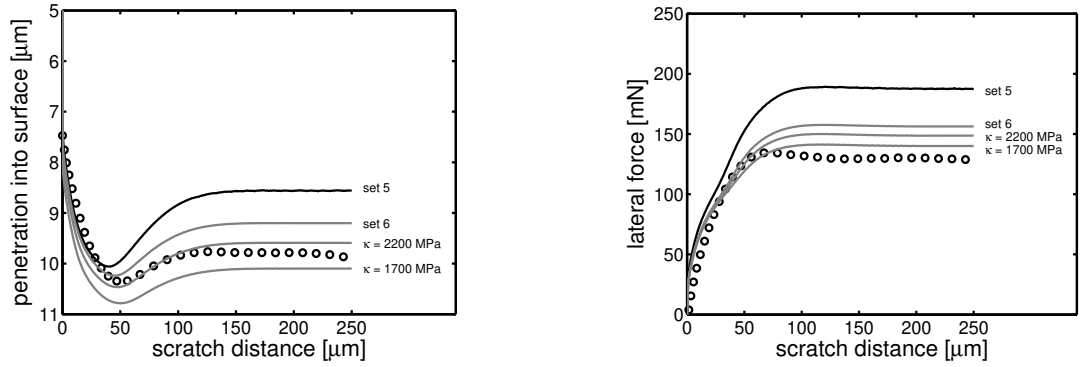

(a) (b)

Figure 19: The effect of 10 vol% voids in the rubber-filled sample, reflected by lowering the bulk modulus to $\kappa = 2700$ MPa (set 6), and the effect of decreasing κ further: penetration into the surface (a) and lateral friction force (b) as a function of scratch distance. Experiments (symbols) at 300 mN normal load and 0.1 µm/s sliding velocity compared to simulation results using different values of κ in parameter set 5.

and $\kappa = 1700$ MPa in combination with paramater set 5, see Figure 19. The Possion's ratios that correspond to these different values of κ are summarized in Table A.5. Lowering κ proves to sufficiently capture the experimental data. Finally, Figure 20 shows that the experimental data are quantitatively modelled in the complete sliding velocity range investigated, if a low value for κ is used. This exercise clearly and illustratively demonstrates the importance of employing proper modeling to interpret experimental results of complex processes.

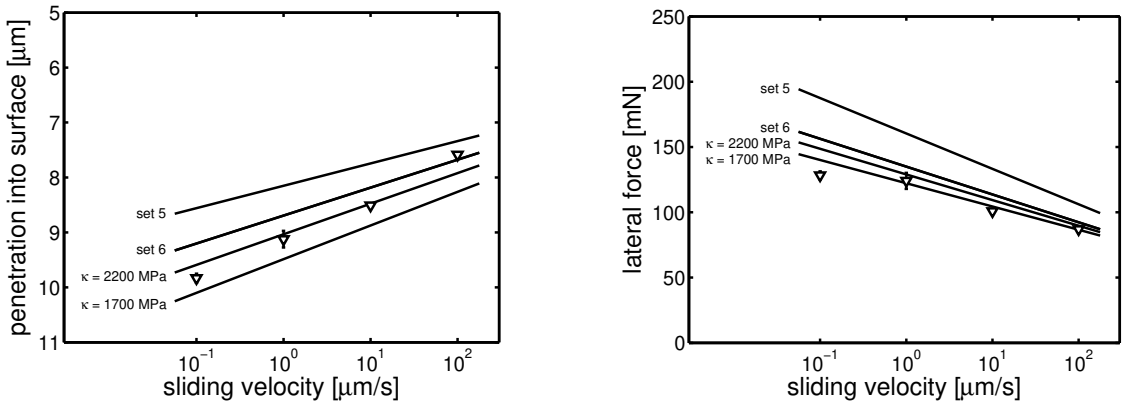

(a) (b)

Figure 20: Penetration into the surface (a) and lateral friction force (b) as a function of scratch velocity for epoxy filled with SR-particles. Experiments (symbols) compared to simulations using $\mu_f = 0.27$ (solid lines) for two different values of bulk modulus κ.

4. Conclusions

The hybrid experimental-numerical approach is successfully used to quantify the frictional response of an unfilled standard epoxy system, over a broad range of sliding velocities and at two different normal loads applied. Finite-element simulations of the single asperity scratch test were performed using material parameters obtained from a previous study. A value of $\mu_f = 0.27$ for the local friction coefficient was found to adequately capture the experimental data, which only slightly deviates from the value of 0.25 previously obtained for polycarbonate [9].

Next the same approach is applied to hard (TiO_2) and soft (rubber) particle-filled epoxy samples, using the numerical method described in [9]. Homogenized material parameters are obtained via RVE-simulations and compression tests. Fillers change the intrinsic mechanical response, and therefore also the scratch response. Hard fillers increase the yield stress and decrease the penetration into the surface, i.e. they enhance scratch resistance, causing the lateral friction force to decrease since less material is moved in front of the indenter tip. This is confirmed by the scratch simulations, using $\mu_f = 0,27$, that quantitatively capture the experiments over the whole sliding-velocity range and for two different normal loads applied.

Soft fillers, in contrast, lower the yield stress and greatly increase the penetration into the surface. An unexpected result is that, although a larger volume of material is addressed, the lateral friction is decreased. This implies a change in friction or local deformation. Simulations confirm that lower values of μ_f, ranging 0.1–0.2, give better predictions, but no unique value of μ_f adequately captures both the surface penetration and the lateral friction response. An alternative explanation, inspired by the relatively large scatter observed in the compression response, is that the rubber fillers tend to agglomerate during the preparation process. For the scratch samples this could cause a surface layer with increased rubber content to form. Scratch simulations employing a 1 µm rubber surface layer, and with again $\mu_f = 0.27$, gave excellent results and, while surface penetration increases, the lateral friction force strongly decreases due to a redistribution of stress, caused by the presence of a rubber layer. However, its existence could not be confirmed by inspecting the cross sections of the samples by SEM and TEM. Instead, serious voiding was found showing in the order of 10% 200–300 nm sized uniformly distributed cavities. Incorporating these voids via a multi-level approach in the modeling proved to result in an interesting macroscopic effect. An increase in penetration depth combined with a decrease in lateral force was predicted over the whole velocity range. Combined with a decreased value of the compressibility κ, it proved quantitative. This exercise witnessed the importance of attempts to interpret experimental results on complex processes with proper modeling.

Acknowledgements

The authors wish to thank AkzoNobel N.V. for their financial support, and Andrew Burgess, Paul Dooling and Gordon Seeley for the many valuable technical discussions that have helped to guide this work. The authors are grateful to Pauline Schmit and Anne Spoelstra for providing the SEM and TEM micrographs.

References

[1] Briscoe BJ, Evans PD, Biswas SK, Sinha SK. The hardnesses of poly(methylmethacrylate). Tribol Int 1996;29(2):93–104. doi:10.1016/0301-679X(95)00045-6.

[2] Briscoe BJ, Pelillo E, Sinha SK. Scratch hardness and deformation maps for polycarbonate and polyethylene. Polym Eng Sci 1996;36(24):2996–3005. doi:10.1002/pen.10702.

[3] Briscoe BJ, Sinha SK. Wear of polymers. Proc Inst Mech Eng [J] 2002;216(6):401–13. doi:10.1243/135065002762355325.

[4] Brostow W, Hagg Lobland HE, Narkis M. Sliding wear, viscoelasticity, and brittleness of polymers. J Mater Res 2006;21(9):2422–8. doi:10.1557/JMR.2006.0300.

[5] Briscoe BJ, Sinha SK. Scratch resistance and localised damage characteristics of polymer surfaces – a review. Materialwiss Werkst 2003;34(10-11):989–1002. doi:10.1002/mawe.200300687.

[6] Mergler YJ, van Kampen RJ, Nauta WJ, Schaake RP, Raas B, van Griensven JGH, et al. Influence of yield strength and toughness on friction and wear of polycarbonate. Wear 2005;258(5-6):915–23. doi:10.1016/j.wear.2004.09.046.

[7] Brostow W, Chonkaew W, Mirshams R, Srivastava A. Characterization of grooves in scratch resistance testing. Polym Eng Sci 2008;48(10):2060–5. doi:10.1002/pen.21085.

[8] van Breemen LCA, Govaert LE, Meijer HEH. Scratching polycarbonate: A quantitative model. Wear 2012;274-275(0):238–47. doi:10.1016/j.wear.2011.09.002.

[9] Krop S, Meijer HEH, van Breemen LCA. Finite element modeling and experimental validation of single-asperity sliding friction of diamond against reinforced and non-filled polycarbonate. Wear 2016;356-357:77–85. doi:10.1016/j.wear.2016.03.014.

[10] Krop S, Meijer HEH, van Breemen LCA. Global and local large-deformation response of sub-micron, soft- and hard-particle filled polycarbonate. J Mech Phys Solids 2016;87:51–64. doi:10.1016/j.jmps.2015.11.005.

[11] Krop S, Meijer HEH, van Breemen LCA. Multi-mode modeling of global and local deformation, and failure, in particle filled epoxy systems. Composites Part A 2016;88:1–9. doi:10.1016/j.compositesa.2016.05.012.

[12] Klompen ETJ, Engels TAP, Govaert LE, Meijer HEH. Modelling of the post-yield response of glassy polymers: Influence of thermomechanical history. Macromolecules 2005;38(16):6997–7008. doi:10.1021/ma050498v.

[13] van Breemen LCA, Klompen ETJ, Govaert LE, Meijer HEH. Extending the EGP constitutive model for polymer glasses to multiple relaxation times. J Mech Phys Solids 2011;59(10):2191–207. doi:10.1016/j.jmps.2011.05.001.

[14] Govaert L, Timmermans P, Brekelmans W. The influence of intrinsic strain softening on strain localization in polycarbonate: modeling and experimental validation. J Engng Mat Technol 2000;122:177–85.

[15] Chen N, Maeda N, Tirrell M, Israelachvili J. Adhesion and friction of polymer surfaces The effect of chain ends. Macromolecules 2005;38(8):3491–503. doi:10.1021/ma047733e.

[16] Knorr DB, Gray TO, Overney RM. Cooperative and submolecular dissipation mechanisms of sliding friction in complex organic systems. J Chem Phys 2008;129(7):074504. doi:10.1063/1.2968548.

[17] Senden DJA, Krop S, van Dommelen JAW, Govaert LE. Rate- and temperature-dependent strain hardening of polycarbonate. J Polym Sci, Part B: Polym Phys 2012;50(24):1680–93. doi:10.1002/polb.23165.

Appendix A. Material parameters

Table A.1: Material parameters for particle-filled epoxy.

filler	set #	G_r [MPa]	κ [MPa]	τ_0 [MPa]	S_a [–]	μ [–]	r_0 [–]	r_1 [–]	r_2 [–]
unfilled	set 1	35	3200	1.5	17.7	0.166	0.977	15	-3.4
10 vol% TiO_2	set 2	63	3675	1.49	17.4	0.219	0.98	50	-4.3
	set 3	44	3675	1.49	16.5	0.219	0.98	20	-2.8
10 vol% SR	set 4	33.2	3645	1.26	17.8	0.153	0.98	14	-3.0
	set 5	26	3645	1.26	16.3	0.153	0.98	15	-2.6
	set 6	26	2700	1.26	16.3	0.153	0.98	15	-2.6

Table A.2: Reference spectrum for epoxy.

mode	$\eta_{0,i,ref}$ [MPa·s]	G_i [MPa]
1	$4.74 \cdot 10^5$	$4.47 \cdot 10^2$
2	$5.79 \cdot 10^3$	$5.77 \cdot 10^1$
3	$1.50 \cdot 10^3$	$5.41 \cdot 10^1$
4	$3.39 \cdot 10^2$	$4.05 \cdot 10^1$
5	$8.41 \cdot 10^1$	$3.33 \cdot 10^1$
6	$2.10 \cdot 10^1$	$2.75 \cdot 10^1$
7	$4.21 \cdot 10^0$	$1.82 \cdot 10^1$
8	$1.21 \cdot 10^0$	$1.74 \cdot 10^1$
9	$2.10 \cdot 10^{-1}$	$1.00 \cdot 10^1$
10	$8.01 \cdot 10^{-2}$	$1.26 \cdot 10^1$
11	$1.69 \cdot 10^{-2}$	$8.79 \cdot 10^0$
12	$7.71 \cdot 10^{-3}$	$1.33 \cdot 10^1$
13	$1.46 \cdot 10^{-3}$	$8.35 \cdot 10^0$
14	$7.18 \cdot 10^{-4}$	$1.36 \cdot 10^1$
15	$1.44 \cdot 10^{-4}$	$9.01 \cdot 10^0$

Table A.3: Reference spectrum for epoxy filled with 10 vol% TiO_2 particles.

mode	$\eta_{0,i,ref}$ [MPa·s]	G_i [MPa]
1	$7.61 \cdot 10^5$	$5.02 \cdot 10^2$
2	$5.15 \cdot 10^3$	$7.31 \cdot 10^1$
3	$5.15 \cdot 10^2$	$2.95 \cdot 10^1$
4	$2.35 \cdot 10^2$	$3.85 \cdot 10^1$
5	$2.50 \cdot 10^1$	$3.05 \cdot 10^1$
6	$3.51 \cdot 10^0$	$2.25 \cdot 10^1$
7	$4.47 \cdot 10^{-1}$	$1.85 \cdot 10^1$
8	$3.18 \cdot 10^{-2}$	$1.28 \cdot 10^1$

Table A.4: Reference spectrum for epoxy filled with 10 vol% SR particles.

mode	$\eta_{0,i,ref}$ [MPa·s]	G_i [MPa]
1	$6.12 \cdot 10^5$	$4.02 \cdot 10^2$
2	$4.14 \cdot 10^3$	$5.96 \cdot 10^1$
3	$4.04 \cdot 10^2$	$2.24 \cdot 10^1$
4	$2.13 \cdot 10^2$	$3.42 \cdot 10^1$
5	$1.01 \cdot 10^1$	$4.38 \cdot 10^0$
6	$2.59 \cdot 10^1$	$2.81 \cdot 10^1$
7	$2.81 \cdot 10^0$	$1.68 \cdot 10^1$
8	$5.18 \cdot 10^{-1}$	$5.25 \cdot 10^0$
9	$3.48 \cdot 10^{-1}$	$1.09 \cdot 10^1$
10	$1.04 \cdot 10^{-1}$	$7.65 \cdot 10^0$
11	$3.82 \cdot 10^{-2}$	$7.90 \cdot 10^0$
12	$1.54 \cdot 10^{-2}$	$7.85 \cdot 10^0$
13	$5.20 \cdot 10^{-3}$	$8.16 \cdot 10^0$
14	$1.48 \cdot 10^{-3}$	$6.71 \cdot 10^0$
15	$5.04 \cdot 10^{-4}$	$7.06 \cdot 10^0$
16	$1.20 \cdot 10^{-4}$	$5.97 \cdot 10^0$
17	$2.58 \cdot 10^{-5}$	$6.59 \cdot 10^0$

Table A.5: Poisson's ratios ν corresponding to the bulk moduli κ used in Figures 18–20.

		set 4–5	set 6		
κ	[MPa]	3645	2700	2200	1700
ν	[–]	0.41	0.39	0.37	0.33